NANO LETTERS
Cite This: Nano Lett. 2018, 18, 202−207
Letter
pubs.acs.org/NanoLett

Magnetically Controlled Atomic−Plasmonic Fano Resonances

Liron Stern,[†] Meir Grajower,[†] Noa Mazurski, and Uriel Levy*,[†]

[†]Department of Applied Physics, The Benin School of Engineering and Computer Science, The Center for Nanoscience and Nanotechnology, The Hebrew University of Jerusalem, Jerusalem 91904, Israel

ABSTRACT: Following the efforts of size reduction and the integration of light and vapor systems, great promise is held in the integration of vapor and confined electromagnetic waves. By confining light to nanoscale dimensions, fundamental properties of light−vapor interactions may vary significantly. For example, the state of polarization may be modified as compared with weakly focused beams. Specifically, in transverse magnetic modes, the existence of a longitudinal field component, which is in quadrature to the transverse field, generates a "circular-like" polarized light. Here, by taking advantage of this very property, we study the interaction of confined light and vapor in a coupled system of plasmons and atomic vapors in the presence of magnetic fields. Our results show that the spectroscopic nature and Fano resonances of the hybrid plasmonic−atomic system are greatly altered. In parallel, we also exploit the existence of the atoms in proximity to the plasmonic mode to probe the polarization state of the electromagnetic field and reveal the longitudinal-to-transverse ratio between the plasmonic modes components in the near field. Interestingly, our system maps the amplitude and phase information of the electromagnetic modes to the spectral domain. As such, combining magnetic fields with the coupled plasmonic−atomic system has the potential for future applications in high spatial resolution magnetometry, near-field vectorial imaging, and magnetically induced switching and tuning.

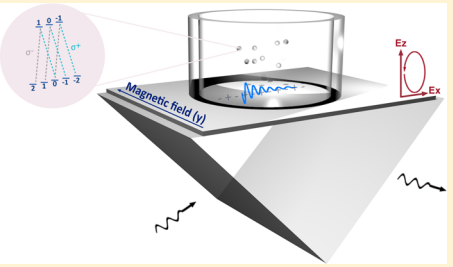

KEYWORDS: *Plasmonics, atomic spectroscopy, Fano resonances, Faraday and Voigt magneto-optic effect*

Recently, we have witnessed a plethora of research in which light−matter interactions are being implemented at the nanoscale, resulting in fascinating and useful effects. For example, localization of light at the nanoscale provides control over its wavelength, which subsequently affects the momentum transfer to matter.[1,2] The electromagnetic density of states is enhanced, leading to shorter lifetimes and faster operation,[3] and the selection rules of atoms may be modified in the vicinity of nanogaps.[4] Furthermore, enhancement of local fields gives rise to strong nonlinearties,[5−7] and striking differences in the spectral response occur in the case of hybridized cavity and atom modes.[8−10] Naturally, polarization is another fundamental property of light, which can be significantly alerted at the nanoscale, with respect to the more conventional free-space configurations. For instance, confined transverse magnetic (TM) propagating modes can have a significant longitudinal electric field component, which is in quadrature to the transverse component. Such interesting polarization features[11] have been investigated in dielectric prisms interacting with argon[12] and, more recently, in nanophotonic whispering-gallery resonators,[13,14] interacting with alkali vapors.

Alkali vapors, such as rubidium (Rb), are being used extensively in several important fields of research such as slow and stored light,[15] nonlinear optics,[16] quantum computation,[17] atomic clocks,[18] and magentometers.[19] Motivated by advanced applications as well as by fundamental research, there is a growing effort toward miniaturizing traditional centimeter-size vapor cells toward the micro- and even the nanoscale. A significant step forward is achieved by incorporating alkali vapors in guided wave configurations such as PhC fibers,[20,21] antiresonant wave-guides,[22] tapered fibers,[23,24] and solid-core waveguides.[2,25−27] Aside from the miniaturization and the high level of integration, these guided wave configurations provide a great enhancement in light matter interactions, allowing new properties, e.g., because of the reduced power threshold for nonlinear interactions. Further confinement of light can be achieved by utilizing metal optics and nanoplasmonics. Plasmonic structures have been already utilized for the purpose of demonstrating a variety of configurations in which light−matter interactions are enhanced.[28] Recently, the interaction of plasmonic structures with cold and hot atoms has been demonstrated.[29−31] Specifically, we recently presented the resonant coupling of surface plasmon resonance and rubidium atomic vapor, giving rise to Fano line shape, which can be controlled all optically.[29] These hybridized systems serve as an outstanding spectroscopic tool capable of probing real and imaginary atomic index of refraction. Furthermore, in such plasmonic systems, it would only natural to exploit the conductive metals to generate localized magnetic and electric fields. This may offer a significant degree of freedom at controlling atoms in the nanoscale. Indeed, the introduction of magnetic fields in such system, gives rise to unique selection rules owing to the presence of longitudinal electric field, which is in 90° phase shift with respect to the more conventional transverse electric field component.[13] As a consequence, the electric field rotates

Received: September 12, 2017
Revised: December 1, 2017
Published: December 14, 2017

DOI: 10.1021/acs.nanolett.7b03912
Nano Lett. 2018, 18, 202−207

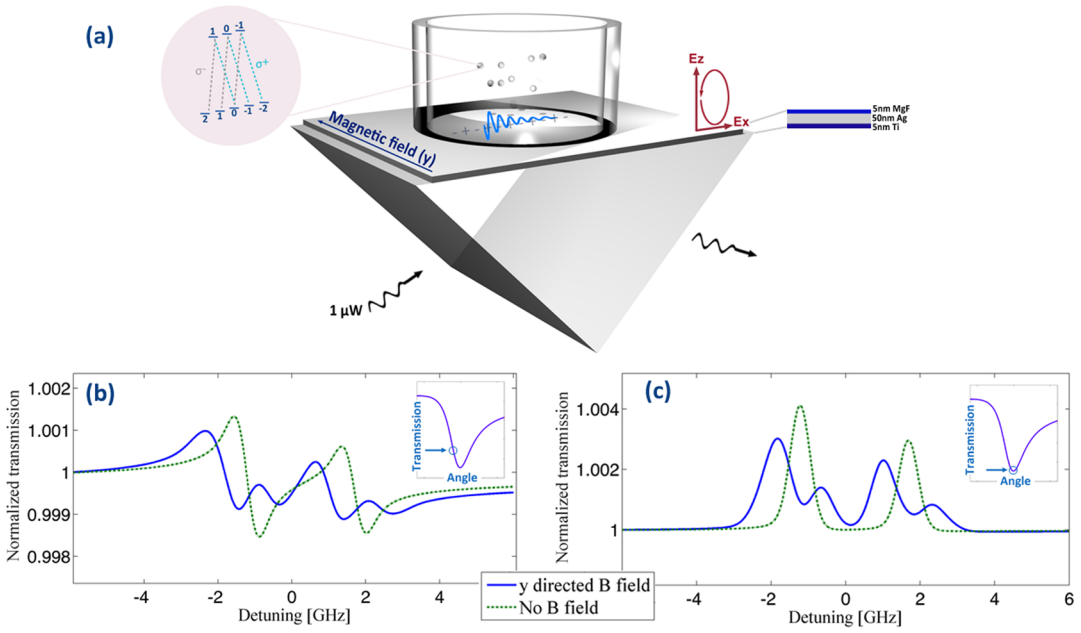

Figure 1. (a) Schematics of the coupled atomic plasmonic device, with magnetic field oriented along the *y*-axis. An atom level scheme showing the Zeeman splitting of the ground and excited states is illustrated. Also shown is the elliptical-like polarization due to the presence of a longitudinal component of electric field. (b) Calculated transmission spectrum of coupled atomic-plasmonic system when both plasmonic and atomic resonances coincide, with (blue curve) and without (green curve) the magnetic field in the direction of the ellipse. (c) The same calculation as in panel b with the atom and plasmon resonance misaligned, leading to asymmetric Fano line-shapes.

elliptically over time giving rise to unconventional selection rules when applying magnetic fields in the direction of this ellipse.

Here, driven by the attractiveness in the coupling of plasmons and atomic vapors, and by the prospects of integrating light, magnetic fields, and vapor in confined and integrated systems, we experimentally reveal the interactions of surface plasmon resonance (SPR) with atomic vapor (Rb) in the presence of magnetic fields. Not only could we observe Fano lineshapes, but also, these lineshapes could be tuned by applying local magnetic fields. Furthermore, we were able to probe the complex atomic evanescent susceptibility (both imaginary and real) under the influence of a magnetic field. Moreover, we observed an inversion of the selection rules associated with the Faraday and the Voigt effects with respect to conventional free space configuration. Finally, as a general extension to evanescent spectroscopy we present a scheme to perform accurate measurements of the local vector electromagnetic field, i.e., the ratio between the longitudinal and the transverse electromagnetic field components. This is a direct consequence of the noninvasive properties of the vapor. Such a scheme can be further expanded to provide a full three-dimensional vector field imaging. Such a platform has the potential for future applications in high spatial resolution magnetometry, near-field vectorial imaging, accurate probing of magnetic surface effects, and magnetically induced switching and tuning.

Materials and Methods. A sketch of the integrated atom-plasmon structure is shown in Figure 1a. An external free space optical mode is converted to a surface plasmon polariton (SPP) mode confined at the interface between metal and vapor, allowing for the vapor to interact with the evanescently decaying SPP mode. The structure is made by coating a prism with 3, 50, and 5 nm layers of Ti, Ag, and MgF_2, respectively; the latter is used to eliminate chemical interaction between the Ag and the atomic vapor. A Pyrex reservoir is epoxy-glued to the structure and is pumped to a pressure below 10^{-7} Torr. Finally, a droplet of ^{85}Rb is inserted, and the reservoir is terminated by a glass-blowing technique. This process results in a small and hand-held device. The device is excited using a ∼1 mm diameter collimated laser beam at the 780 nm wavelength, around the D2 transition. We heat the cell using resistors to a temperature of ∼40 °C, which defines the cold spot. It is important to maintain this spot far from the metal to diminish vapor condensation. To avoid atomic saturation, we maintained the optical power to be around 1 μW.

As we have presented in a previous work,[29] the coupling between a SPR and Rb is a highly convenient platform to study Fano resonances. Hereby, we briefly describe such hybridized resonances. The plasmonic−atomic system presented in Figure 1a (in the absence of a magnetic field) is illuminated by a 780 nm laser, having a transverse magnetic (TM) polarization. For a given incident frequency, such a device exhibits a resonance with respect to the incident angle. In the frequency domain, each incident angle corresponds to a resonant frequency with a relative broad (a few hundred nanometers in spectral width) line-width. Because the atomic resonance has line-width orders of magnitude smaller than the SPR resonance, the coupling of the two modes gives rise to the well-known Fano resonances,[32] with line shape that is highly dependent on the frequency detuning between both resonances. Moreover, by examining the line shape one can identify the excitation order (excitation of the SPR and coupling to the atoms or vice versa). Indeed, it has been verified experimentally that the SPR−Rb system exhibits clear Fano resonance, which has a direct dependence on the angle of incidence of light. For instance, when the plasmonic and atomic resonances coincide, one gets a peak in transmission, as is evident in the green line in Figure 1c. In contrast, when the plasmonic resonance is detuned from the

DOI: 10.1021/acs.nanolett.7b03912
Nano Lett. 2018, 18, 202−207

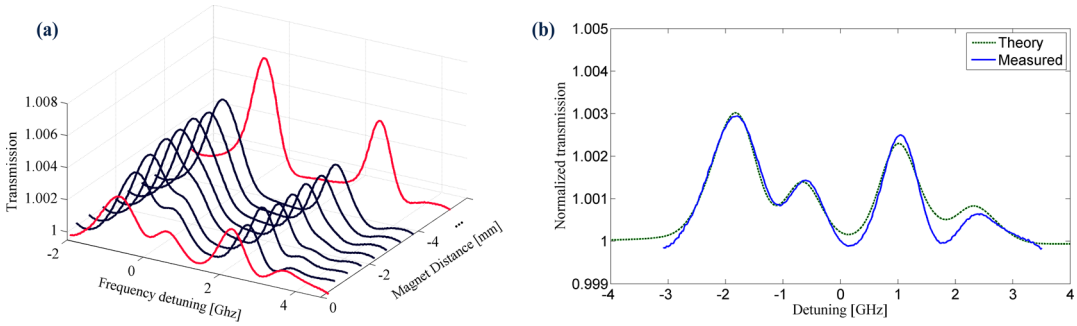

Figure 2. (a) Transmission spectra for different distances between the magnet and the prism, when the magnetic field is directed in the plane of the ellipse. The two red curves represent the cases of vanishing magnetic field (large distance) and maximal magnetic field (nearly zero distance). (b) Calculated and measured spectrum of coupled atomic−plasmonic structures in the case in which the magnet is placed next to the prism and the direction of the magnetic field is perpendicular to the ellipse.

atomic resonances one gets a dispersion-like line-shape, as illustrated in green in Figure 1b.

Next, we turn to describe the influence of the magnetic field on such hybridized Fano resonances. First, one should note that the SPP wave, being a TM mode, has two electric field components: a transverse field (directed along the z axis in Figure 1a) and a longitudinal component (directed along the x axis in Figure 1a). These two field components are 90° out of phase each in respect to the other, and therefore, the electric field rotates elliptically in the xz plane. This is in contrast to the free-space configuration. We thus refer to this type of vector field as "elliptical-like polarization" (ELP). Consequently, this unique field will alter the selection rules one encounters in standard free space configurations. For instance, the free-space Faraday configuration, in which the direction of propagation and a magnetic field are co-aligned (and perpendicular to the plane of electric field), induces selection rules of $\Delta m_F = \pm 1$ (m_F being the projection of the total angular momentum of the atom F. Such transitions are coined σ_+ and σ_-, respectively). In free-space Voigt configuration, in which the magnetic field is perpendicularly aligned with the direction of light propagation and not necessarily perpendicular to the electric field component, the selection rules are generally $\Delta m_F = 0 \pm 1$ ($\Delta m_F = 0$ transitions are coined π transitions). In contrast, for the surface Plasmon mode, co aligning the magnetic field and the propagation direction (x axis) will result in selection rules of $\Delta m_F = 0$ and ± 1. And yet, aligning the magnetic field along the xz plane, i.e, perpendicular to the ellipse plane induces $\Delta m_F = \pm 1$ transitions. Thus, it turns out that for the plasmonic system the Faraday and Voigt configurations reverse their roles, i.e., the Faraday configuration turns into a Voigt configuration, and vice versa.

To quantify the splitting ratio between the σ_+ and σ_- transitions when the magnetic field axis is aligned with the ellipse (y-axis), we express the ELP in a left and right circular polarization base, corresponding to the two different possible transitions. In general, we can decompose an elliptical polarization as $|\psi\rangle = a \cdot |\mathbf{TR}\rangle + ib \cdot |\mathbf{LO}\rangle = (a - b)/\sqrt{2}|R\rangle + (a + b)/\sqrt{2}|\mathbf{L}\rangle$. Here, a and b are the amplitude of the transverse ($|\mathbf{TR}\rangle$) and the longitudinal $|\mathbf{LO}\rangle$ electric field components, respectively, and $|\boldsymbol{R}\rangle$ and $|\boldsymbol{L}\rangle$ are the right- and left-hand circularly polarized bases, respectively. According to this decomposition, the ratio between right- and left-hand circular polarization is given by the ratio $(a - b)/(a + b)$. For our specific case, this ratio is 2/3. This number has been estimated by the well-known ratio between the SPPs electric field components, namely $i(k_x/k_z)^{1/2}$ (where $k_{x/z}$ are the plasmonic wavenumbers in the x/z direction) as well as by a finite element method commercial software (COMSOL). We use the convention that $\boldsymbol{\sigma}^+$ transitions are excited by circularly polarized light, which turns clockwise in the direction of propagation (left circularly polarized light), and $\boldsymbol{\sigma}^-$ transitions are excited by circularly polarized light, which turns counterclockwise in the direction of propagation (right circularly polarized light).

Next, we find the overall response of the combined system. Our procedure is based on the formalism of attenuated total internal reflection,[33−35] which we modify to account for our configuration, including the magnetic field. We start by calculating the vapor susceptibility, considering thermal velocity, quenching at the interface and the momentum of the plasmonic mode. Doppler and transit time broadening are both considered. The SPP mode momentum is found within the layered structure that includes: prism/Ti/Ag/MgF_2/air. We ignore the influence of the vapor on the SPP mode momentum, which is justified due to the low vapor density. This approach was successfully used and shown outstanding agreement with measurements.[2,29,34−36] Knowing the SPP momentum, it is now possible to calculate the spatial profile and the SPP mode index. Considering the wavelength of interest ∼780 nm the mode is found to decay at a distance of 500 nm from the interface, and the SPP mode index was found to be ∼1.03. To find how the applied magnetic field is affecting the properties of the hybrid atom-plasmon mode, we calculate both of the oscillator strengths as well as the transition energies of ^{85}Rb D2 hyperfine manifold in the mixed Zeeman and Paschen−Back regime (for a few hundred Gauss, the upper hyperfine transitions are in the Paschen−Back regime, and the lower transitions are in the Zeeman regime) and use them to calculate the susceptibility for σ_+, σ_-, and π transitions. Next, we apply the following procedure: (a) we calculate the ratio between σ_+ and σ_- transitions, (b) we use a five-layer model and extract the SPP mode transmission coefficient with Rb susceptibility as a parameter, and (c) we apply the reflection coefficient to each susceptibility separately, i.e, $T \approx (a - b)^2 T_{spp}(\sigma_-) + (a + b)^2 T_{spp}(\sigma_+)$. Based on this procedure, we plot in panels b and c of Figure 1 the calculated plasmonic−atomic system in the presence of an external magnetic field (300 G, at 40 °C) applied in the direction of the ellipse. Figure 1b is calculated for the case in which the plasmonic and atomic resonances are aligned, whereas Figure 1c is calculated for the case of a energy mismatch between the plasmonic and atomic resonances. This

DOI: 10.1021/acs.nanolett.7b03912
Nano Lett. 2018, 18, 202−207

mismatch can be obtained experimentally simply by rotating the prism in respect to the illuminating beam. In both figures, we plot the transmission with and without the applied magnetic field. Clearly, it can be seen that each transition is split into two different components, with a ratio corresponding to the square of $(a - b)/(a + b)$. In the case in which the resonances are aligned, as plotted in Figure 1b, the plasmonic−atomic system inverts transmission dips (observed in a conventional atomic system) into peaks; see Figure 1b and the dashed green curve. However, when magnetic field is applied, each of the two observed peaks is split into two separated peaks, which are detuned from the original peak. In contrast (Figure 1c), the case of misaligned resonances yields in general an asymmetric Fano line shape (also related to the imaginary index of refraction of the atoms). Furthermore, the applied magnetic field splits these line shapes into two spectrally shifted asymmetric line shapes having the above-mentioned ratio. Thus, we can probe the magnetically affected real andimaginary parts of indices of refraction, observe the existence of a longitudinal electric field component, and measure the ratio between the transverse and longitudinal electric fields of the plasmonic mode.

Results and Discussion. We now elaborate on the experimentally measured results obtained with the hybrid plasmon-atom device in the presence of applied magnetic field. First, we scan the D2 manifold of ^{85}Rb by exciting the plasmonic−atomic system when both resonances are spectrally aligned. In parallel, we apply a permanent magnetic field perpendicular to the ellipse, as described above, under similar conditions in Figure 1b. We vary the magnetic field strength by changing the distance between the magnet and the surface.

Figure 2a demonstrates the measured transmitted spectra of the integrated structure while varying the magnetic field strength. Clearly, as we increase the magnetic field, the splitting of the two components increases and is easier to be observed, as the two overlapping peaks are resolvable (spectrum plotted in red, at the minimal distance possible). To compare the measured spectrum to the calculated one, we calibrate the magnetic strength by measuring the frequency detuning between the two peaks, and use the density of atoms as a free parameter. We plot the calculated and the measured spectrum in Figure 2b and find excellent agreement between the two curves (i.e., replication of the earlier mentioned ratio between right- and left-hand circular polarization is given by $(a - b)/(a + b)$. The small discrepancy in the signal strength is probably the result of a Fabry−Perot effect due to reflections from the interfaces, which gives rise to a nonuniform (in frequency) background.

Following the previous result, we now apply the magnetic field in a different direction, i.e., the direction of propagation. In a conventional configuration, this would correspond to the known Farady effect, and according to the selection rules, only the $\Delta m_F = \pm 1$ transitions are allowed. However, in the case of guided wave configuration with light matter interactions originated by the evanescent field, all three possible transitions of $\Delta m_F = 0$ and ± 1 are allowed, resembling the Voigt configuration. For our plasmonic mode, this will result in two symmetrically shifted lineshapes corresponding to the transverse electric field components decomposed into equal σ+ and σ- transitions, and a π transition, corresponding to the longitudinal electric field component. Through the application of moderate magnetic fields (as in our case), the existence of π transition in addition to the other two transitions generally broadens the line-shape in a symmetric fashion. Thus, we expect to observe a line shape composed of the two shifted σ_+ and σ_- transitions and the broadened π transition. Indeed, we observed such an effect, as can be seen in Figure 3. The

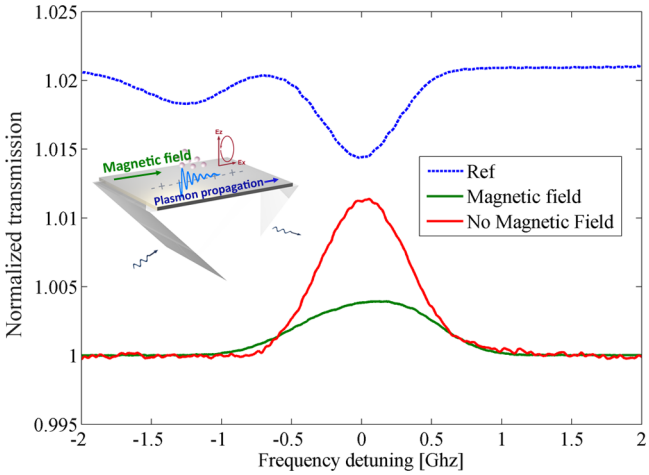

Figure 3. . Measured Spectrum of the coupled atomic−plasmonic system. The magnetic field is aligned with the light propagation direction. Both resonances coincide spectrally.

magnetically affected plasmonic−atomic spectrum is plotted in a blue line, while the response in the absence of magnetic field is presented in a green line. A reference natural Rb cell is presented in red. Indeed, the magnetically influenced spectrum (blue) is symmetrically broadened as anticipated.

Parallel to the demonstration of the spectroscopic features of hybridized lineshapes with magnetic field, we now highlight the general capability of evanescent spectroscopy with the presence of magnetic fields. Such a line shape, accompanied by the line shape presented in Figure 2b, can be combined as a noninvasive method, allowing us to accurately map the plasmonic near field components. Furthermore, such a scheme can be generalized to three dimensions by using three different magnetic fields along the three orthogonal axes.

We now turn into studying the regime in which the atomic and plasmonic resonant frequencies do not coincide. To do so, we slightly (within half of a degree) rotate the prism in respect to the incident beam. By doing so, as we have shown in the past,[29] an asymmetrical Fano line shape is obtained. This Fano line shape is presented in Figure 4 (red line). Similar to Figure 3, we once again plot the reference of a natural Rb lines (blue line). Finally, we plot the measured spectrum obtained by applying a magnetic field perpendicular to the ellipse's plane (green line). In comparison to the case in which no magnetic field is applied (red line), we now observe the splitting of the curve into two components, in which the magnitude as well as the slope of each dispersive line shape components is different owning to the different ratio of left and right circular polarization content in the plasmonic mode. Such a spectrum is very similar to the spectrum presented in Figure 2c, albeit with a slightly weaker magnetic field.

Conclusions. To summarize, we have studied the interactions of surface plasmon resonances and Rb vapor under the application of external magnetic fields. Taking advantage of the strong longitudinal field component of the plasmonic mode, we could observe selection rules that are very different as compared to the case of free-space propagation.

DOI: 10.1021/acs.nanolett.7b03912
Nano Lett. 2018, 18, 202−207

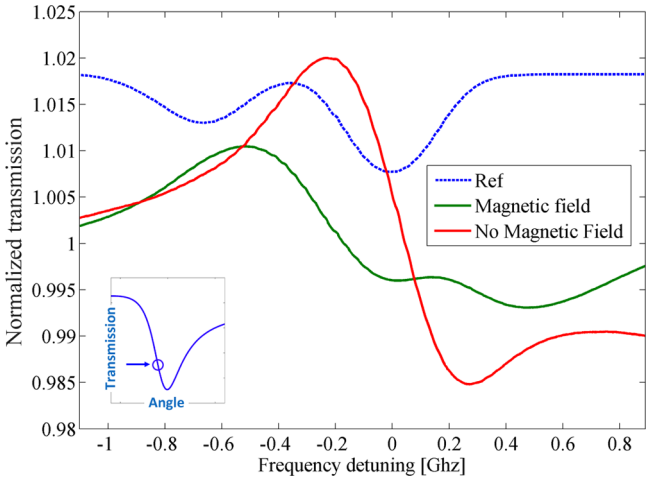

Figure 4. Spectrum of coupled atomic−plasmonic structure. Magnetic field is applied normal to the ellipse. Atomic and plasmonic resonances are misaligned.

Specifically, the conventional Faraday effect turns into the Voigt effect and vice versa. In contrast to plane wave propagation, here the polarization plane is not perpendicular to the propagation direction. This is a direct consequence of the strong field localization, giving rise to enhanced longitudinal electric field component. Interestingly, as our plasmonic−atomic system is capable of probing the two components of refractive index in the complex plane, we can now probe these values in the presence of magnetic fields and learn some more about the properties of the hybrid system, including the enhancement of effects such as slow light and damping. Furthermore, by applying an external magnetic field, we demonstrated switching and tuning the transmission properties of the system.

It is well-known that circular polarizations are desired in many light−vapor interactions. Unfortunately, due to difference in effective index between the two transverse field components of a guided mode, a circularly polarized light is not an Eigen mode of a rectangular waveguide. However, as being pointed out recently,[13] a TM guide mode can support a circular-like polarization due to its longitudinal field. In this regard, our plasmonic system provides an even-better solution because it only supports a TM mode. While our current structure supports an elliptical-like polarization, it can be modified to support a pure circularly like polarization by tailoring the properties of the dielectric and metallic layers. In such a case, it would be possible to shift the hybrid lineshapes, and obtain better on-to-off ratios. It should be emphasized that other photonic structures, such as TM waveguides, whisper-gallery microresonators,[13,14] and hollow-core photonic crystal fibers[37] as well as plasmonic devices such as hybrid wave guides and v-groove plasmonic wave guides[38] may also support such quasi-elliptical modes, albeit differing in their overall response that is reported in this work (i.e., do not have angle-dependent resonance coupling). In such devices, the ellipticity of these modes can be controlled by tailoring the physical dimension and material composition of the structure.

Furthermore, such a platform may be appealing for the purpose of constructing nonreciprocal devices, such as a plasmonic isolators, exploiting the high Verdet coefficient of Rb.[39] An additional general merit of introducing magnetic fields in evanescent spectroscopic platforms, such our hybrid SPR−Rb system, is the ability to distinguish between the different E-field components associate with the plasmonic mode. As a result, we have shown that it is indeed possible to measure the two E-field components related with the SPP mode with high level of accuracy in both amplitude and phase. Generally, the imaging of near-field polarization components has been accomplished using a tailored near field optical microscope.[40] This technique provides unprecedented polarization maps, yet at the expense of slow scanning and perturbation to the electromagnetic field, particularly around resonance.[41] Thus, mapping the electromagnetic polarization components into the spectral domain may hold promise in 3D noninvasive imaging applications. Another inherent advantage of using magnetic fields in plasmonic devices is the ability to exploit the conductive plasmonic structures for the purpose of generating magnetic fields. Due to the small size of these structures, switching the magnetic fields can be achieved in very short time scales. Finally, as the plasmonic mode decays at the submicron scale, such a platform may be possible to achieve high spatial resolution magnetometry. Keeping in mind that by incorporating antirelaxation coating with evanescent fields resolutions at the pT level have been demonstratede,[42] a plasmonic−atomic platform for magnetometry seems appealing.

AUTHOR INFORMATION

Corresponding Author

*E-mail: ulevy@cc.huji.ac.il.

ORCID

Liron Stern: 0000-0002-4588-110X

Meir Grajower: 0000-0003-4973-1800

Uriel Levy: 0000-0002-5918-1876

Funding

The authors acknowledge funding from the Europe Research Council (ERC-LIVIN).

Notes

The authors declare no competing financial interest.

ACKNOWLEDGMENTS

The authors acknowledge A. Stern, Y. Barash and B. Levy at AccuBeat for using their vacuum facilities.

REFERENCES

(1) Matsudo, T.; Takahara, Y.; Hori, H.; Sakurai, T. *Opt. Commun.* **1998**, *145*, 64−68.

(2) Stern, L.; Desiatov, B.; Goykhman, I.; Levy, U. *Nat. Commun.* **2013**, *4*, 1548.

(3) Anger, P.; Bharadwaj, P.; Novotny, L. *Phys. Rev. Lett.* **2006**, *96*, 113002.

(4) Kim, H. Y.; Kim, D. S. *Nanophotonics* **2017**, *7*, 229−236.

(5) Kauranen, M.; Zayats, A. V. *Nat. Photonics* **2012**, *6*, 737−748.

(6) Metzger, B.; Hentschel, M.; Schumacher, T.; Lippitz, M.; Ye, X.; Murray, C. B.; Knabe, B.; Buse, K.; Giessen, H. *Nano Lett.* **2014**, *14*, 2867−2872.

(7) Stern, L.; Desiatov, B.; Mazurski, N.; Levy, U. *Nat. Commun.* **2017**, *8*, 14461.

(8) González-Tudela, A.; Huidobro, P. A.; Martín-Moreno, L.; Tejedor, C.; García-Vidal, F. J. *Phys. Rev. Lett.* **2013**, *110*, 126801.

(9) Manjavacas, A.; de Abajo, F. J. G.; Nordlander, P. *Nano Lett.* **2011**, *11*, 2318−2323.

(10) Christ, A.; Tikhodeev, S. G.; Gippius, N. A.; Kuhl, J.; Giessen, H. *Phys. Rev. Lett.* **2003**, *91*, 183901.

(11) Van Mechelen, T.; Jacob, Z. *Optica* **2016**, *3*, 118.

(12) Kawalec, T.; Józefowski, L.; Fiutowski, J.; Kasprowicz, M. J.; Dohnalik, T. *Opt. Commun.* **2007**, *274*, 341−346.

DOI: 10.1021/acs.nanolett.7b03912
Nano Lett. 2018, 18, 202−207

(13) Junge, C.; O'Shea, D.; Volz, J.; Rauschenbeutel, A. *Phys. Rev. Lett.* **2013**, *110*, 213604.
(14) Shomroni, I.; Rosenblum, S.; Lovsky, Y.; Bechler, O.; Guendelman, G.; Dayan, B. *Science* **2014**, *345*, 903−906.
(15) Camacho, R. M.; Vudyasetu, P. K.; Howell, J. C. *Nat. Photonics* **2009**, *3*, 103−106.
(16) Venkataraman, V.; Saha, K.; Gaeta, A. L. *Nat. Photonics* **2012**, *7*, 138−141.
(17) Lvovsky, A. I.; Sanders, B. C.; Tittel, W. *Nat. Photonics* **2009**, *3*, 706−714.
(18) Knappe, S.; Shah, V.; Schwindt, P. D. D.; Hollberg, L.; Kitching, J.; Liew, L.-A.; Moreland, J. *Appl. Phys. Lett.* **2004**, *85*, 1460−1462.
(19) Budker, D.; Romalis, M. *Nat. Phys.* **2007**, *3*, 227−234.
(20) Benabid, F.; Couny, F.; Knight, J. C.; Birks, T. A.; Russell, P. S. J. *Nature* **2005**, *434*, 488−491.
(21) Slepkov, A. D.; Bhagwat, A. R.; Venkataraman, V.; Londero, P.; Gaeta, A. L. *Phys. Rev. A* **2010**, *81*, 053825.
(22) Yang, W.; Conkey, D. B.; Wu, B.; Yin, D.; Hawkins, A. R.; Schmidt, H. *Nat. Photonics* **2007**, *1*, 331−335.
(23) Spillane, S. M.; Pati, G. S.; Salit, K.; Hall, M.; Kumar, P.; Beausoleil, R. G.; Shahriar, M. S. *Phys. Rev. Lett.* **2008**, *100*, 233602.
(24) Hendrickson, S.; Lai, M.; Pittman, T.; Franson, J. *Phys. Rev. Lett.* **2010**, *105*, 173602.
(25) Ritter, R.; Gruhler, N.; Pernice, W.; Kübler, H.; Pfau, T.; Löw, R. *Appl. Phys. Lett.* **2015**, *107*, 41101.
(26) Ritter, R.; Gruhler, N.; Pernice, W. H. P.; Kübler, H.; Pfau, T.; Löw, R. *New J. Phys.* **2016**, *18*, 103031.
(27) Stern, L.; Zektzer, R.; Mazurski, N.; Levy, U. *Laser Photon. Rev.* **2016**, *10*, 1016−1022.
(28) Schuller, J. A.; Barnard, E. S.; Cai, W.; Jun, Y. C.; White, J. S.; Brongersma, M. L. *Nat. Mater.* **2010**, *9*, 193−204.
(29) Stern, L.; Grajower, M.; Levy, U. *Nat. Commun.* **2014**, *5*, 4865 DOI: 10.1038/ncomms5865.
(30) Stehle, C.; Bender, H.; Zimmermann, C.; Kern, D.; Fleischer, M.; Slama, S. *Nat. Photonics* **2011**, *5*, 494−498.
(31) Aljunid, S. A.; Chan, E. A.; Adamo, G.; Ducloy, M.; Wilkowski, D.; Zheludev, N. I. *Nano Lett.* **2016**, *16*, 3137−3141.
(32) Fano, U. *Phys. Rev.* **1961**, *124*, 1866−1878.
(33) Nienhuis, G.; Schuller, F.; Ducloy, M. *Phys. Rev. A: At., Mol., Opt. Phys.* **1988**, *38*, 5197−5205.
(34) Zhao, K.; Wu, Z. *Phys. Rev. A: At., Mol., Opt. Phys.* **2005**, *71*, 12902.
(35) Kondo, R.; Tojo, S.; Fujimoto, T.; Hasuo, M. *Phys. Rev. A: At., Mol., Opt. Phys.* **2006**, *73*, 62504.
(36) Ritter, R.; Gruhler, N.; Pernice, W.; Kübler, H.; Pfau, T.; Löw, R. *Appl. Phys. Lett.* **2015**, *107*, 041101.
(37) Noble, R. J.; Spencer, J. E.; Kuhlmey, B. T. *Phys. Rev. Spec. Top.–Accel. Beams* **2011**, *14*, 121303.
(38) Smith, C. L. C.; Stenger, N.; Kristensen, A.; Mortensen, N. A.; Bozhevolnyi, S. I. *Nanoscale* **2015**, *7*, 9355−9386.
(39) Weller, L.; Kleinbach, K. S.; Zentile, M. A.; Knappe, S.; Hughes, I. G.; Adams, C. S. *Opt. Lett.* **2012**, *37*, 3405−3407.
(40) Rotenberg, N.; Kuipers, L. *Nat. Photonics* **2014**, *8*, 919−926.
(41) Abashin, M.; Levy, U.; Ikeda, K.; Fainman, Y. *Opt. Lett.* **2007**, *32*, 2602.
(42) Zhao, K. F.; Wu, Z. *Appl. Phys. Lett.* **2008**, *93*, 101101.

DOI: 10.1021/acs.nanolett.7b03912
Nano Lett. 2018, 18, 202−207